Analysis of the Notch Tip Damage Zone in Biaxially Oriented Polypropylene

J. SNYDER, A. HILTNER,* and E. BAER

Department of Macromolecular Science and Center for Applied Polymer Research, Case Western Reserve University, Cleveland, Ohio 44106

SYNOPSIS

The circular notch tip damage zone in biaxially oriented polypropylene has been analyzed using a thickness correction to the elastic stress distribution for a sharp-notched tension specimen. The size and shape of the damage zone as a function of applied stress followed a critical mean stress criterion, independent of specimen thickness. Also, the damage zone only grew while σ_3 was greater than zero. Close observations of sections through the damage zone revealed that the circular zone, which consisted of many delamination crazes, had a distinctive pattern when viewed across the thickness direction. Large crazes grew into a triangular pattern with smaller crazes in between them. The shape development of the triangular profile as well as the smaller crazes was explained using a stress-redistribution argument. The growth path of the delamination crazes in the x–z plane appeared to be in a direction perpendicular to the direction of σ_3. © 1994 John Wiley & Sons, Inc.

INTRODUCTION

Recent studies of the effect of biaxial orientation on the prefracture damage zone in polypropylene showed that the wedge-shaped damage zone in unoriented polypropylene changed to a circular-shaped zone as the level of orientation increased to 80%.[1] Furthermore, it was revealed that the damage zone in this highly oriented material consisted of many delamination crazes. This form of damage was very different than that observed in the unoriented material and reflected the high anisotropy between the rolled directions and thickness direction.

The analysis of the damage zone in unoriented polypropylene at temperatures below the glass transition showed that the narrow wedge-shaped damage zone followed the modified Dugdale model that predicted both the damage zone length and notch-opening displacement based on basic material properties.[2] The Dugdale model, which is a one-dimensional analysis of a yield zone, was very useful in describing a damage zone with a very high length-to-width ratio that resembled a reinforced crack. In the case of the highly oriented material, the length-to-width ratio was not as large and a one-dimensional analysis was not adequate.

An alternative approach to an analysis of the damage zone is to determine the stress condition at the boundary of the damage zone. With this approach, it was shown that the cavitation damage mechanisms in poly(vinyl chloride) blends and in the styrene–acrylonitrile copolymer (SAN) at a semicircular notch followed an iso-mean stress condition.[3,4] This approach used the exact two-dimensional elastic stress distribution to calculate the plane strain stress state at the damage zone boundary. It was assumed that at the boundary the real stress distribution had not deviated far from elastica.

The goal of this article was to analyze the circular damage zone in 80% oriented polypropylene using an elastic stress analysis approach. It was anticipated that the results of this analysis would help determine the controlling microdeformation mechanisms and the criteria for damage zone growth in this system.

EXPERIMENTAL

Polypropylene sheet was cross-rolled as described previously to achieve a final level of orientation of

* To whom correspondence should be addressed.

Journal of Applied Polymer Science, Vol. 52, 231–241 (1994)
 CCC 0021-8995/94/020231-11

80%, defined as the percentage reduction in thickness (t), and calculated using the equation $100x(t_i - t_f)/t_i$.[1] Starting stock thicknesses were chosen to produce final rolled thicknesses of 1.3 and 5.1 mm. ASTM D638, type D, dog-bone tension specimens with dimensions of 60 mm gauge length, 13 mm width, and a 1.3 mm or 5.1 mm final thickness were cut from the sheets. Specimens were polished using 800, 1200, and 2400 grit wet sandpaper to remove surface damage from the rolling process. A single 1 mm edge notch was slowly cut at room temperature using a fresh razor blade.

Single-edge notched tension testing was conducted on an Instron 1123 testing instrument equipped with a liquid nitrogen-cooled environmental chamber at a crosshead speed of 0.1 mm per min. The prefracture damage ahead of the notch was recorded during loading using a 35 mm camera with a telephoto lens.

Several specimens were loaded to predetermined stress levels and unloaded for microtome sectioning. Microtoming was conducted at room temperature using glass knives. The specimens were sectioned through the thickness perpendicular to the notch in the direction of tensile loading. Slicing started at the notch tip and proceeded forward through the damage zone. Micrographs were taken of the remaining specimen every 20 μm. Using this technique, the length of damage zone features was measured and the exact shape of these features could be determined.

RESULTS AND DISCUSSION

Elastic Stress Distribution

The elastic stress distribution ahead of the sharp notch in a single-edge notch specimen was solved by Irwin for the region close to the notch tip.[5] Theocaris and Spiropoulos extended this solution to larger distances from the notch tip by including higher-order terms to the series solution.[6] This expanded series solution was utilized with a correction by Creager and Paris for crack-tip blunting[7] to calculate the stresses at the damage-zone boundary. The first three terms of this solution for the stresses were

$$\sigma_x = \frac{K_i}{2(\pi a)^{1/2}}\left[\left(\frac{r}{2a}\right)^{-1/2}\cos\left(\frac{\theta}{2}\right)\left[1 - \sin\left(\frac{\theta}{2}\right)\times\sin\left(\frac{3\theta}{2}\right)\right] - \left(\frac{r}{2a}\right)^{-1/2}\frac{\rho}{2r}\cos\left(\frac{3\theta}{2}\right) + \frac{3}{2}\left(\frac{r}{2a}\right)^{1/2}\cos\left(\frac{\theta}{2}\right)\left[1 + \sin^2\left(\frac{\theta}{2}\right)\right] + \cdots\right] \quad (1)$$

$$\sigma_y = \frac{K_I}{2(\pi a)^{1/2}}\left[\left(\frac{r}{2a}\right)^{-1/2}\cos\left(\frac{\theta}{2}\right)\left[1 + \sin\left(\frac{\theta}{2}\right)\times\sin\left(\frac{3\theta}{2}\right)\right] + \left(\frac{r}{2a}\right)^{-1/2}\frac{\rho}{2r}\cos\left(\frac{3\theta}{2}\right) + \frac{3}{2}\left(\frac{r}{2a}\right)^{1/2}\cos^3\left(\frac{\theta}{2}\right) + \cdots\right] \quad (2)$$

$$\tau_{xy} = \frac{K_I}{2(\pi a)^{1/2}}\left[\left(\frac{r}{2a}\right)^{-1/2}\sin\left(\frac{\theta}{2}\right)\cos\left(\frac{\theta}{2}\right)\cos\left(\frac{3\theta}{2}\right) - \left(\frac{r}{2a}\right)^{-1/2}\frac{\rho}{2r}\sin\left(\frac{3\theta}{2}\right) - \frac{3}{4}\left(\frac{r}{2a}\right)^{1/2}\times\sin\left(\frac{\theta}{2}\right)\cos\left(\frac{\theta}{2}\right) + \cdots\right] \quad (3)$$

where $K_I = \sigma_0 Y\sqrt{a}$, $Y = 1.99 - 0.41(a/W) + 18.7(a/W)^2 - 38.48(a/W)^3 + 53.85(a/W)^4$; σ_0 is the externally applied stress; a, the notch length; ρ, the notch radius; and W, the specimen width, with r and θ being the radial coordinates. From these solutions, the principal stresses σ_1 and σ_2 were obtained from the relationships

$$\sigma_1, \sigma_2 = \frac{\sigma_x + \sigma_y}{2} \pm \sqrt{\left(\frac{\sigma_x - \sigma_y}{2}\right)^2 + \tau_{xy}^2} \quad (4)$$

For the analysis, three possible stress states were considered: In the plane stress condition, σ_3 is zero, whereas in the case of plane strain, $\sigma_3 = \nu(\sigma_1 + \sigma_2)$. The plane strain assumption is appropriate for very thick specimens with small-scale yielding, but in cases when the distance from the notch tip (i.e., damage zone size) is comparable to the specimen thickness, small-scale yielding is lost and the stress state is intermediate between plane strain and plane stress. The extent of this condition is often referred to as the degree of plane strain and is given a value between one for pure plane strain and zero for the plane stress condition. In this third situation, a value of the degree of plane strain (DPS) is defined from the real σ_3 as

$$\text{DPS} \equiv \frac{\sigma_3}{\nu(\sigma_1 + \sigma_2)} \quad (5)$$

Several finite element analysis programs have been used to calculate the three-dimensional stress distribution ahead of a sharp notch.[8-10] The finite element solutions show that the degree of plane strain decreases from a value of one at the notch tip to zero at a radial distance (r) equal to one-half the thickness (t) of the specimen ahead of the notch

tip. For intermediate positions, the curves that describe the degree of plane strain (DPS) empirically follow the equation.[8-10]

$$\text{DPS} \simeq \left(1 - \frac{2r}{t}\right)^{2.9} \tag{6}$$

Using this result, the value of σ_3 was calculated as $\sigma_3 = \nu(\sigma_1 + \sigma_2) \times \text{DPS}$ at any point in the stress field to correct for finite specimen thickness. The value of σ_3 is also dependent on the position through the specimen thickness (z-direction), but for the current analysis, the stress state was considered only along the central plane of the thickness. The mean stress was also calculated from the principal stresses by

$$\sigma_m = \frac{(\sigma_1 + \sigma_2 + \sigma_3)}{3} \tag{7}$$

Iso-stress contours of σ_1, σ_2, σ_3, and σ_m were calculated from these equations for both the plane strain case (DPS = 1) and the plane strain case modified for finite specimen thickness (DPS $\leq$ 1). The calculated σ_1 and σ_2 iso-stress contours were the same for both cases by definition and are plotted in Figure 1 together with the σ_3 and σ_m contours. Large differences were found in the shape and magnitude of the σ_3 contours when the plane strain and modified plane strain cases were compared. In the modified plane strain case, the σ_3 contour was shifted in the x-direction toward the notch and extended behind the notch tip. The magnitude of σ_3 in the modified case approached the plane strain value at the notch tip, but quickly dropped as the distance from the notch tip increased. The σ_m iso-stress contours were not affected by the modification as much as were the σ_3 contours. The shape of the σ_m contour

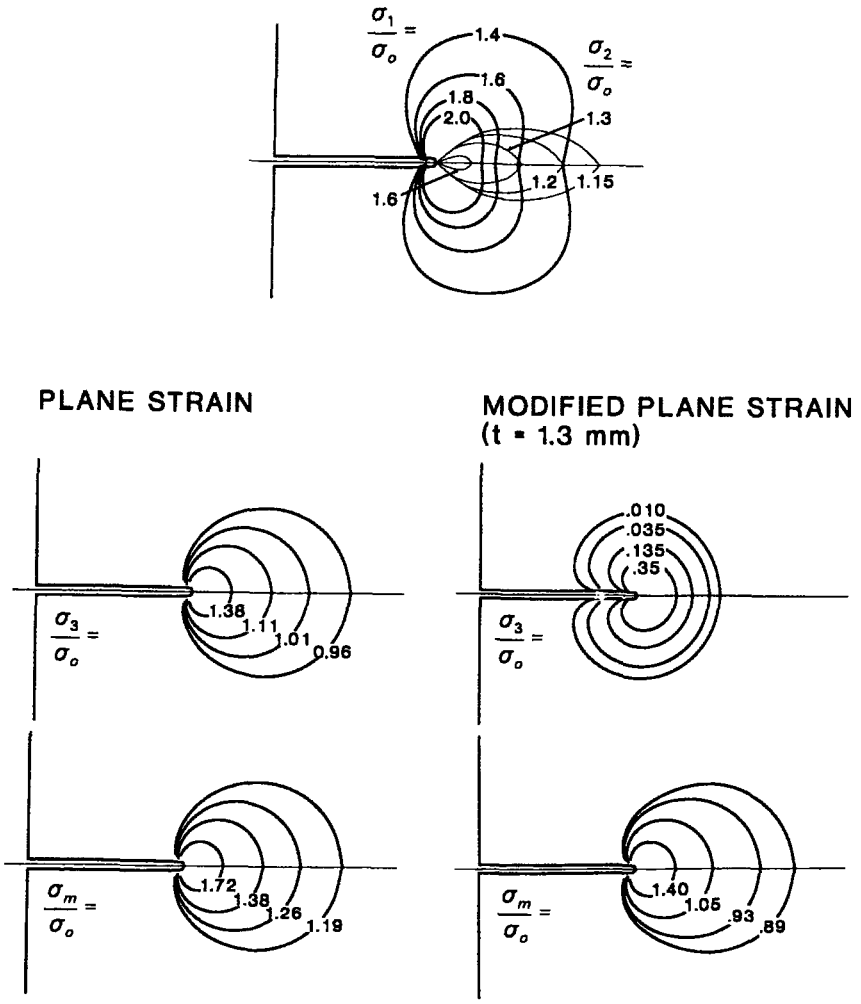

Figure 1 Iso-stress contours for the three principal stresses and mean stress for plane strain conditions and plane strain modified for decreasing σ_3 with distance from the notch tip.

was similar to the plane strain case and the magnitude was only slightly lower.

Craze Growth Conditions

Craze boundaries in the x–y plane were determined from microtomed sections. Data from several of the larger crazes in the damage zone at two stress levels, 0.5 and $0.7\sigma_y$, are plotted in Figure 2. The data showed that the shape of the crazes remained very nearly circular regardless of applied stress or position in the thickness direction. These shapes resembled the mean stress contours of both the plane strain and modified plane strain calculations, and it was not possible from the craze shape to differentiate between the two approaches.

Using the solutions for the stress distribution, the principal stresses were calculated at the points on the boundary of the largest central craze for several applied stress levels. The calculated plane strain mean stress at points on the damage zone boundary is plotted in Figure 3(a) as a function of angle. Along the circular craze boundary, there was good agreement with a constant mean stress condition in the plane strain case, but the mean stress value that best fit the data was different for each applied stress level. The mean stress condition was independent of applied stress only when the degree of plane strain (modified plane strain approach) was taken into account [Fig. 3(b)]. The σ_m values that best fit the data from both the plane strain and modified plane strain approaches are compared in Table I. Individual modified plain strain σ_m values were within 1 standard deviation of the average up to an applied stress of $0.8\sigma_y$. At the higher stress of $0.9\sigma_y$, the σ_m value deviated most likely because of the start of crack growth.

The effect of thickness was also examined since a thickness dependency would be additional evidence that modification of the plane strain approach was necessary. Qualitatively, a larger damage zone was observed for any stress level when the thickness of 80% biaxially oriented polypropylene was increased from 1.3 to 5.1 mm. The mean stress was calculated at the point where the damage zone boundary intersected the x-axis. The plane strain values, in-

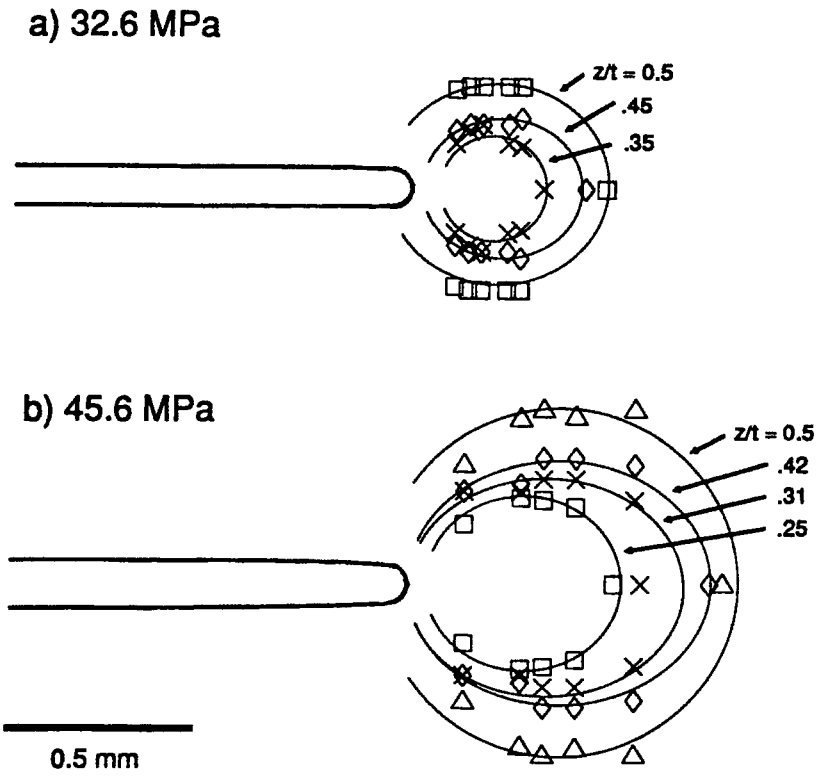

Figure 2 The results of slice measurements to construct the shape of individual crazes located at several positions in the thickness of the specimen. The largest craze is very near the center of the specimen thickness: (a) stress level of $0.5\sigma_y$ (32.8 MPa); (b) $0.7\sigma_y$ (45.6 MPa).

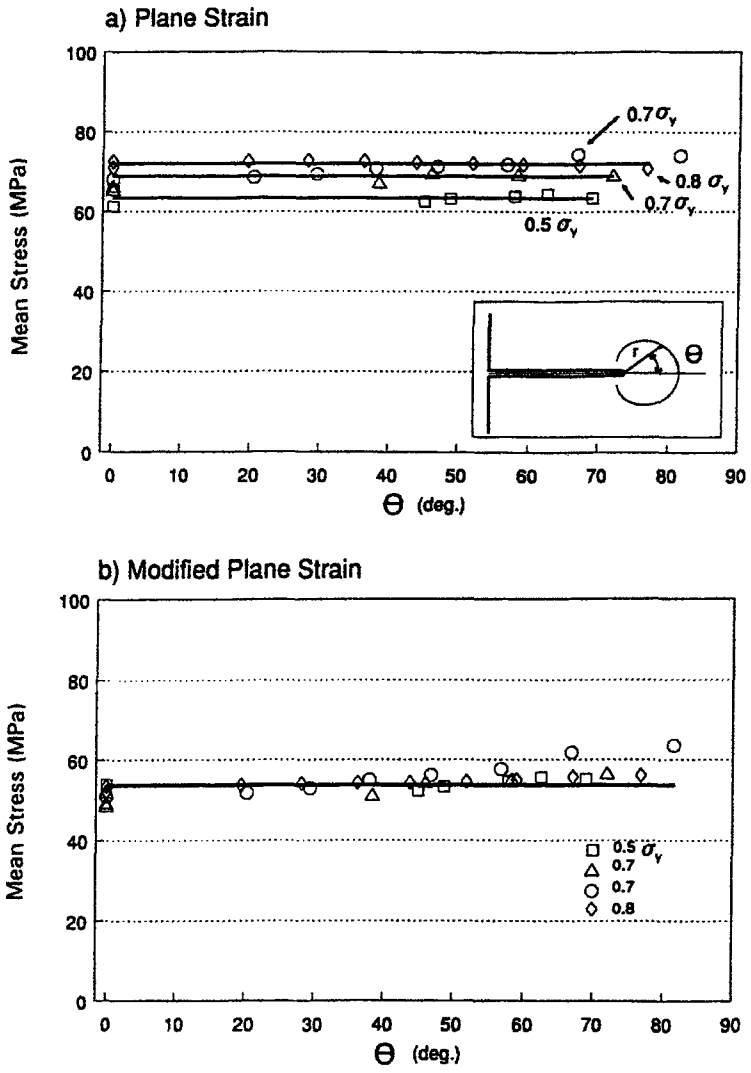

Figure 3 Calculated mean stress along the craze tip boundary: (a) plane strain; (b) plane strain with the finite thickness correction.

cluded in Table I, were lower than the values for 1.3 mm thick material while also varying with stress level. Use of the modified plane strain calculation gave mean stress values for the thick material that were in line with those for thin material and again removed the dependency on stress level.

The fit of the σ_m contours with the experimentally determined boundary of the damage zone is shown in Figures 4 and 5. In Figure 4, the average mean stress value from the plane strain calculations of 68.8 MPa (Table I) was used to obtain the iso-mean stress contour at three applied stress levels. Similar calculations in Figure 5 were made for the modified plane strain case using an average mean stress of 53.8 MPa. Comparison of the two figures clearly showed that the best fit with a unique value of the mean stress condition at the boundary of the largest craze was obtained when the plane strain solution was corrected for finite thickness. Since this value was not dependent on the applied stress level or thickness, 53.8 MPA was taken as the critical mean stress ($\sigma_{m,c}$) for growth of the delamination crazes in 80% biaxially oriented polypropylene.

Figure 6(a) and (b) show the effect of the finite thickness correction on σ_3. The correction shifted the values of σ_3 from the 50–60 MPa range for plane strain down to the 2–30 MPa range. Figure 6(b) shows that σ_3 was not constant along the damage zone boundary but increased from a low value where the zone intersected the x-axis ($\Theta = 0$), which was the point on the zone boundary furthest from the notch, to much higher values at larger angles which

Table I Calculated Stresses Along the Perimeter of the Large Center Craze

	Applied Stress (MPa)	σ/σ_y	No Thickness Effect σ_m (MPa)	With Thickness Effect σ_m (MPa)
Thin specimens (1.3 mm)	32.6	0.5	63.4 ± 1.9%	53.4 ± 3.7%
	45.6	0.7	67.8 ± 2.3%	52.3 ± 5.4%
	45.6	0.7	71.0 ± 3.1%	56.2 ± 7.6%
	50.7	0.8	72.1 ± 0.8%	54.1 ± 1.7%
	58.6	0.9	82.2[a]	60.3[a]
Thick specimens (5.1 mm)	32.4	0.5	54.8	50.9
	44.6	0.7	62.1	52.0
Average			68.5	53.8

[a] Data from this stress level is not included in the average.

were progressively closer to the notch tip. Figure 6(b) also shows that the calculated values of σ_3 were lower than the plane strain values even when conditions were closest to the plain strain stress state, e.g., when the specimen was thick or in thin specimens when the damage zone was small.

Examination of the final fracture surface showed that the longest craze did not grow beyond one-half

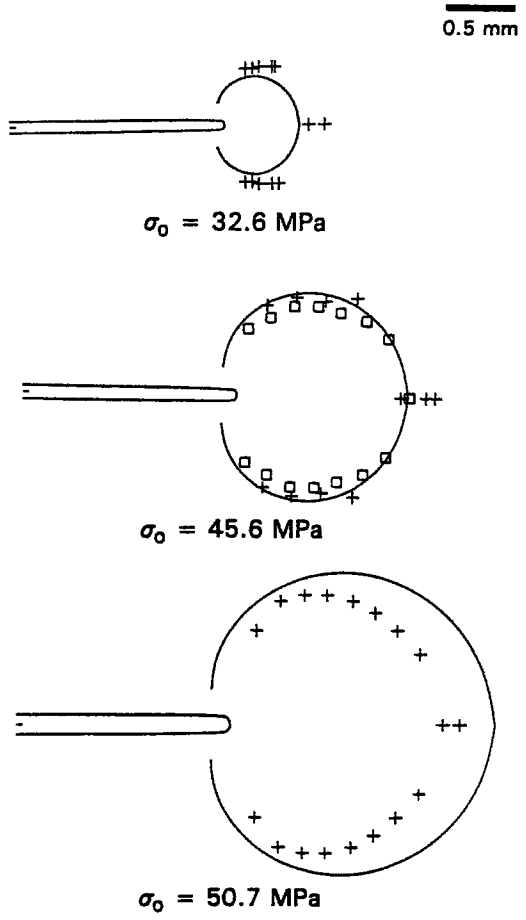

Figure 4 Comparison of the measured points along the craze tip boundary with the σ_m = 68.5 MPa stress contour, assuming plane strain.

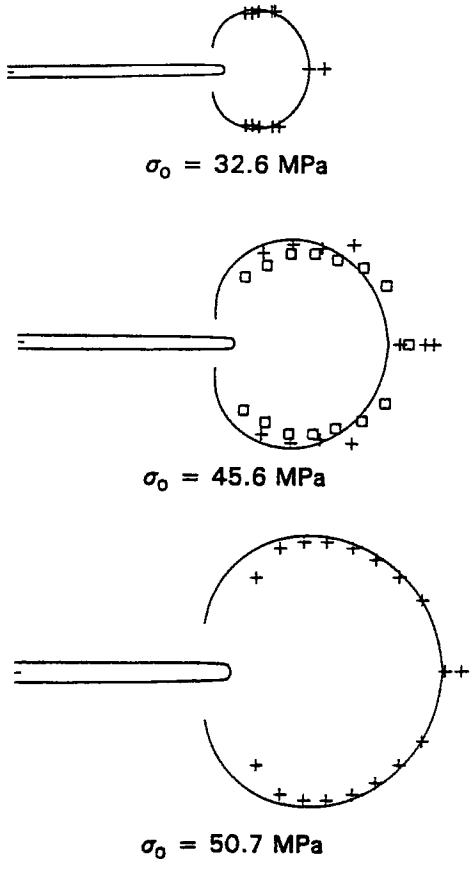

Figure 5 Comparison of the measured points along the craze tip boundary with the σ_m = 53.6 MPa stress contour, assuming plane strain with the finite thickness correction.

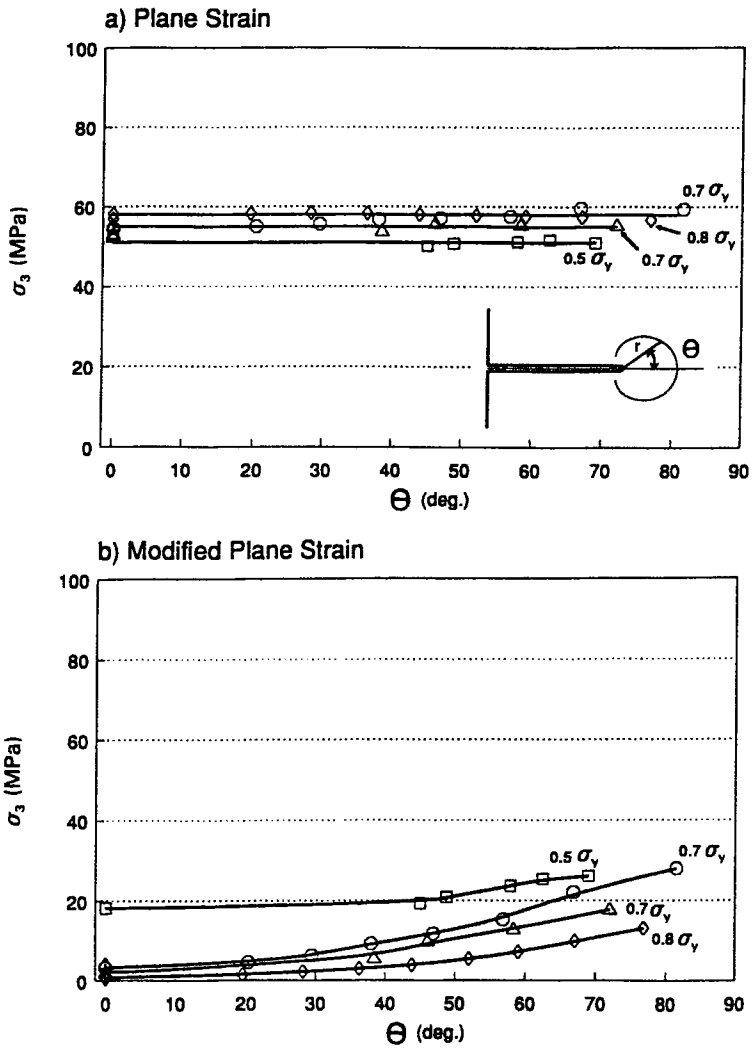

Figure 6 Calculated σ_3 along the craze tip boundary: (a) plane strain; (b) plane strain with the finite thickness correction.

of the thickness of the specimen with both 1.3 and 5.1 mm thicknesses. From eq. (6), this was the distance from the notch tip at which σ_3 dropped to zero. This emphasized the importance of σ_3 in the growth of the delamination crazes and revealed a second criterion for craze growth: that σ_3 be greater than zero.

The result of a critical mean stress condition at the craze boundary implied that voiding at the craze tip was the controlling micro-mechanism for the growth of the delamination crazes. Using this critical mean stress, a critical volume strain was calculated using the equation

$$V_c = \frac{\sigma_{m,c}}{K} = \frac{3(1-2\nu)\sigma_{m,c}}{E} \qquad (8)$$

where K is the bulk modulus, and E, Young's modulus. The critical volume strain in this case, based on a Young's modulus of 4.1 GPa and a Poisson's ratio of 0.365, was 1.0%. This magnitude of critical volume strain was similar to that found for crazing in the styrene–acrylonitrile copolymer (SAN), which ranged from 0.82 to 0.97%,[3] for crazing in polycarbonate, 1.2%,[11] and at the boundary of the stress-whitened zone in PVC blends where the critical volume strain was 0.8%.[4]

Stress Redistribution

A complex pattern of craze lengths was revealed by microtoming through the center of the damage zone parallel to the notch (Fig. 7). The largest crazes

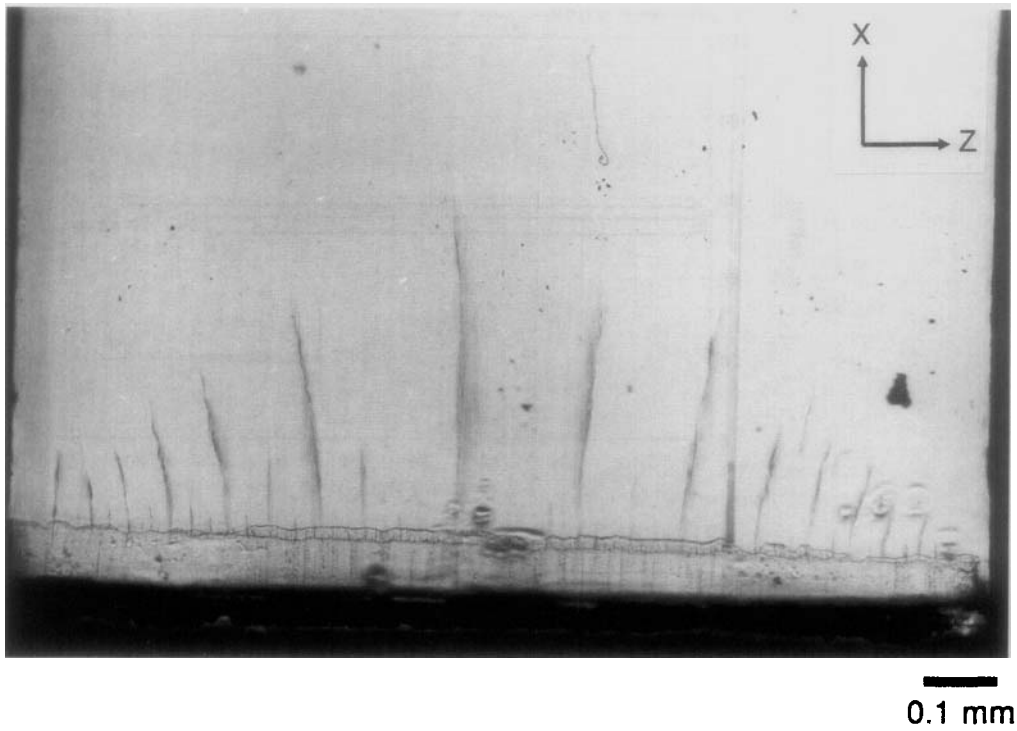

Figure 7 An optical micrograph of a section through the damage zone of a 1.3 mm-thick specimen loaded to $0.7\sigma_y$ at $-40°C$.

created a distinctive profile across the specimen thickness with the longest craze at the center of the cross section and progressively shorter ones toward either surface. At this stress level, the longest craze was about 0.35 mm long, which corresponded to the length of the circular damage zone when it was photographed *in situ* from the side. The shape of the craze profile depended on the applied stress level and specimen thickness. At low stresses or in thick specimens, the craze length was reasonably uniform across most of the thickness (Fig. 8) but quickly dropped at each surface. At high stresses or in thin specimens, the profile was triangular with the longest craze approaching one-half of the thickness of the sheet.

The triangular shape of the profile crazes could not be explained by either the σ_m or the σ_3 stress contours through the thickness (z-direction). Exact solutions for these stress contours were not available but could be estimated from published finite element analysis results.[9] These results predict that the magnitude of σ_3 drops from a maximum level at the center of the section to zero at the surface with a major part of the stress drop occurring near the surface, whereas the magnitude of σ_m decreases only about 10% at the surface.

The concept of stress redistribution as described by Shin et al. was used to explain the triangular profile of the large crazes at high stress and low thickness.[3] Stress redistribution in the thickness direction resulted when a longer craze closer to the center of the section relieved the triaxial stress state between it and the surface. Consequently, the region between the longer craze and the surface resembled a thinner sheet with a lower DPS. A profile craze growing between the longer craze and the specimen edge grew in a redistributed stress field with a lower σ_3; the length of the craze was determined by the critical mean stress condition in the redistributed stress field. Stress redistribution between the larger crazes affected the smaller crazes between them. The magnitude of the stress redistribution effect was dependent on both the applied stress level and the specimen thickness. At low stress levels and in thick specimens, the stress redistribution was smallest, resulting in a fairly uniform craze length through the thickness except near the surfaces. In contrast, redistribution was maximized at high stress levels and thin specimens that produced the triangular craze profile.

Shorter crazes appeared approximately midway between the large profile crazes at stress levels of $0.7\sigma_y$ or above. Again, the length of these crazes depended on applied stress level, but the length was generally equal to one-half to three-quarters of the distance between the larger profile crazes to either

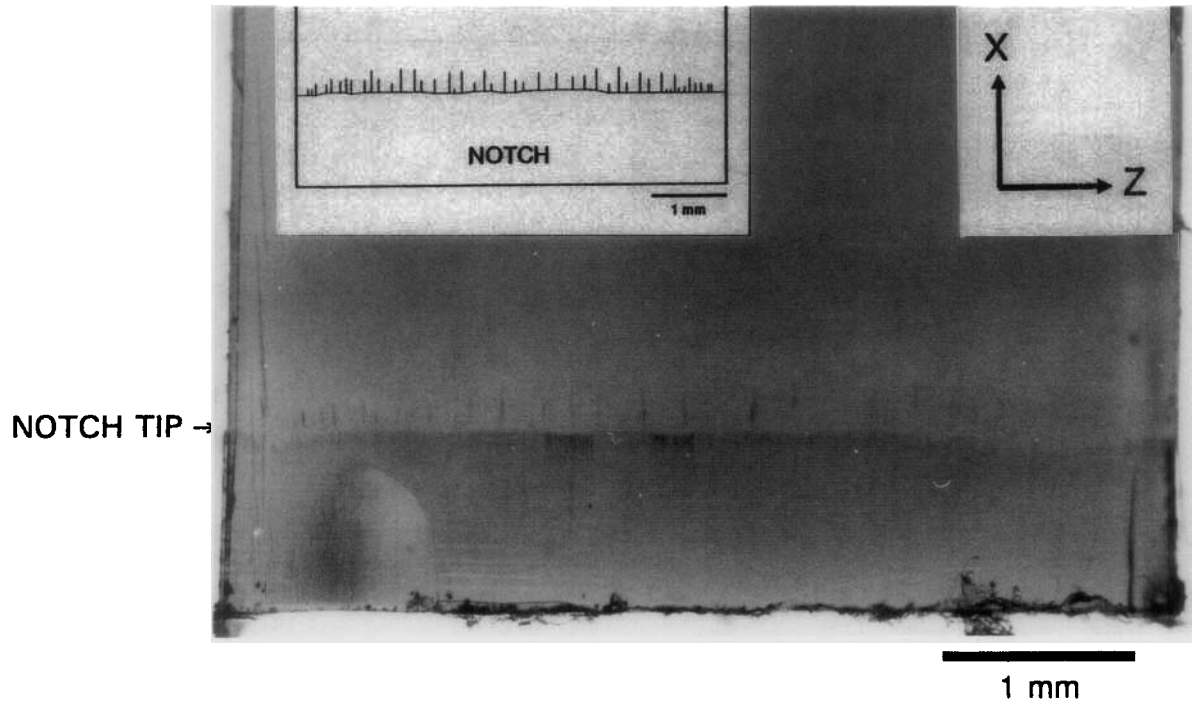

Figure 8 An optical micrograph of a section through the damage zone of a 5.1 mm-thick specimen loaded to 0.5 σ_y at −40°C. The sketch was made from several higher magnification micrographs.

side. The region between the major crazes probably behaved on a local level as a much thinner sheet. When the local stresses reached a critical level, a delamination craze formed in each of these smaller regions, thus relieving the local triaxiality. Careful examination of Figure 7 revealed an entire hierarchy of shorter crazes growing midway between longer crazes until the spacing between crazes was about 50 μm, which was on the same size scale as the thickness of the flattened spherulites.

Craze Paths in the Thickness Direction

The craze paths in the thickness direction of the 80% cross-rolled material in Figure 7 distinctly curved toward the surface of the specimen as the crazes grew from the notch tip. The paths of the larger crazes in one-half of the cross section in Figure 7 are plotted in Figure 9(a) with the deviation of the larger crazes from a straight path plotted in Figure 9(b) as a function of distance from the center line of the specimen. This figure shows that the craze curvature increased with distance from the center line of the specimen thickness.

When the orientation process flattened and aligned the spherulites, weak planes were created parallel to the plane of the sheet. It was expected that delamination crazing would occur along these weak planes, and the observed curvature of the craze path was unanticipated. However, a curved craze path has been found in the damage zone of unoriented polypropylene, where crazes followed a path perpendicular to the maximum local principal stress, which is the minor principal stress trajectory.[2] This was also the case for surface crazing in SAN where the surface crazes followed the principal stress trajectory ahead of a semicircular notch.[3] Although crazing in both of these isotropic solids grew in a different plane from the delamination crazes of biaxially oriented polypropylene, similar trajectory considerations were applied.

In the isotropic plane stress case, the angle of the trajectory (β) at any point ahead of the notch was calculated from the equation

$$\beta = \frac{1}{2}\tan^{-1}\left[\frac{\sigma_y - \sigma_x}{2\tau_{xy}}\right] \tag{9}$$

where σ_x, σ_y, and τ_{xy} are the local stresses. In the anisotropic case of biaxially oriented polypropylene, crazing occurred in the weak x–z plane and was strongly influenced by σ_3. It would not be surprising if craze growth in the x–z plane occurred perpen-

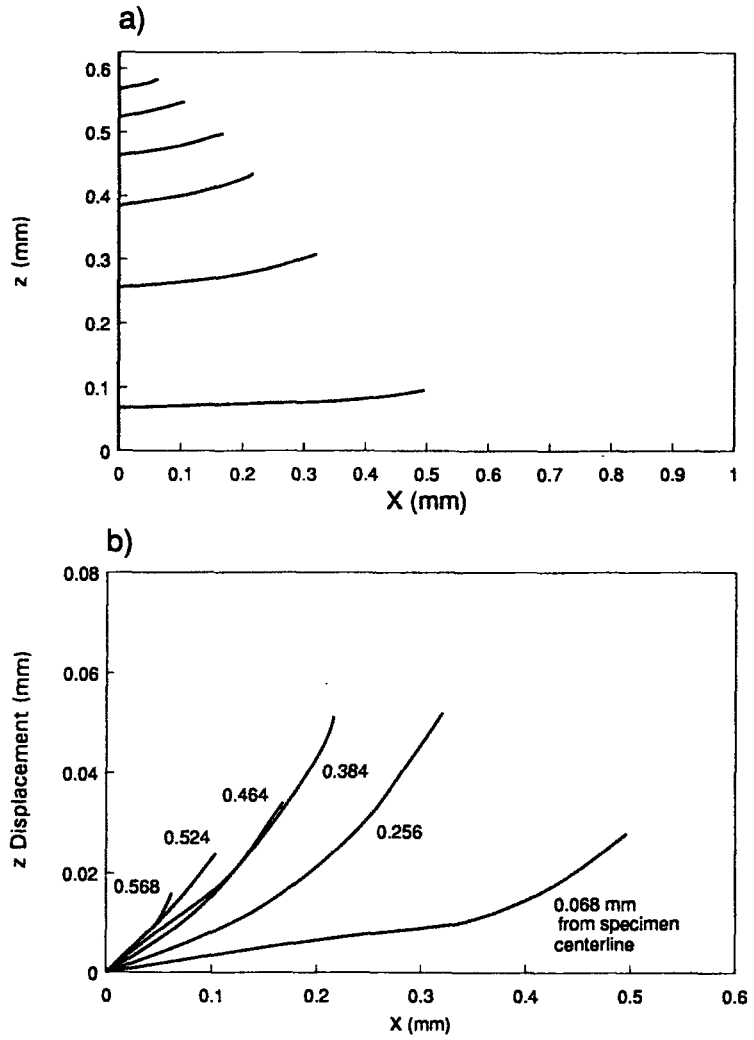

Figure 9 Plots of (a) the craze path and (b) the craze curvature of delamination crazes that grew in the thickness of the specimen in Figure 7.

dicular to σ_3, which would be the σ_2 trajectory. The direction of σ_3 has not been addressed in detail in the literature, but is assumed to be in the z-direction. Evidence to suggest that this assumption is not accurate can be found in the results of three-dimensional finite element analysis of the sharp notch.[8-10] These results show that the x–z shear stresses increase from zero at the center of the specimen thickness to nontrivial values near the surface. The presence of these shear stresses means that the direction of σ_3 is at an angle to the z-direction. This angle (γ) can be calculated using

$$\gamma = \frac{1}{2}\tan^{-1}\left[\frac{\sigma_x - \sigma_z}{2\tau_{xz}}\right] \qquad (10)$$

where σ_x, σ_z, and τ_{xz} are the local stresses. As the magnitude of the shear stress increases, so does the angle of σ_3. Although the σ_2 trajectories in the x–z plane cannot be quantitatively determined, from eq. (10), it is seen that they would curve toward the surface from the notch root with the amount of curvature increasing from the center to the surface. Qualitatively, this produces the same type of curvature observed with delamination crazing in Figure 9(a) and (b).

CONCLUSIONS

Analysis of the damage zone of the 80% cross-rolled polypropylene was achieved by using a thickness correction to the elastic stress distribution for a sharp-notched tension specimen. The results of the analysis showed the following:

1. The size and shape of the damage zone follow a critical mean stress criterion of 53.6 MPa

independent of applied stress up to $0.8\sigma_y$ and independent of sample thickness. A second criterion for craze growth is that σ_3 be greater than zero.

2. In the thickness direction, the delamination crazes grow into a triangular profile with the longest craze growing to a maximum length of one-half of the thickness of the specimen. This is the distance at which σ_3 drops to zero regardless of the applied stress.
3. Smaller crazes grow between the larger crazes to a maximum length of slightly greater than one-half of the distance between the larger crazes. The triangular shape of the craze profile and the existence of the small crazes are attributed to the redistribution of stresses caused by the presence of the larger crazes.
4. Craze growth paths ahead of the notch tip follow the minor principal stress trajectories, similar to the growth of crazes in the unoriented material but in a different plane.

The authors thank the National Science Foundation, Polymers Program, Grant No. DMR91-00300, for the generous support of this work.

REFERENCES

1. J. Snyder, A. Hiltner, and E. Baer, *J. Appl. Poly. Sci.*, **52,** 217 (1994).
2. J. Snyder, A. Hiltner, and E. Baer, *J. Mater. Sci.*, **27,** 1969 (1992).
3. E. S. Shin, A. Hiltner, and E. Baer, *J. Appl. Poly. Sci.*, **46,** 213 (1992).
4. A. Tse, E. S. Shin, A. Hiltner, and E. Baer, *J. Mater. Sci.*, **26,** 2823 (1991).
5. G. R. Irwin and J. A. Kies, *Weld. J. Res. Suppl.*, **33,** 1935 (1954).
6. P. S. Theocaris, *Fracture,* **1,** 707 (1984).
7. M. Creager and P. Paris, *Int. J. Fract. Mech.*, **3,** 247 (1967).
8. T. Nakamura and D. M. Parks, *J. Appl. Mech.*, **55,** 805 (1988).
9. I. D. Parsons and J. F. Hall, *Eng. Fract. Mech.*, **33,** 45 (1984).
10. D. M. Tracey, *Nucl. Eng. Design,* **26,** 282 (1974).
11. R. P. Kambour, M. A. Vallance, E. A. Farraye, and L. A. Grimaldi, *J. Mater. Sci.*, **13,** 1427 (1978).

Received September 21, 1992
Accepted December 21, 1992